MOLECULAR AND CELLULAR BIOLOGY, Jan. 2011, p. 351–364 Vol. 31, No. 2
0270-7306/11/$12.00 doi:10.1128/MCB.00259-10

Mammalian Polycomb-Like Pcl2/Mtf2 Is a Novel Regulatory Component of PRC2 That Can Differentially Modulate Polycomb Activity both at the *Hox* Gene Cluster and at *Cdkn2a* Genes▽

Xiangzhi Li,[1] Kyo-ichi Isono,[1]† Daisuke Yamada,[1]† Takaho A. Endo,[2] Mitsuhiro Endoh,[1,3] Jun Shinga,[1] Yoko Mizutani-Koseki,[1] Arie P. Otte,[4] Miguel Casanova,[5] Hiroshi Kitamura,[1] Takehiko Kamijo,[6] Jafar Sharif,[1] Osamu Ohara,[1] Tetsuro Toyada,[2] Bradley E. Bernstein,[7] Neil Brockdorff,[5] and Haruhiko Koseki[1,3]*

RIKEN Research Center for Allergy and Immunology[1] and RIKEN Bioinformatics and Systems Engineering Division,[2] 1-7-22 Suehiro, Tsurumi-ku, Yokohama 230-0045, Japan; JST, CREST, 1-7-22 Suehiro, Tsurumi-ku, Yokohama 230-0045, Japan[3]; Swammerdam Institute for Life Sciences, University of Amsterdam, Kruislaan 406, 1098 SM Amsterdam, Netherlands[4]; Department of Biochemistry, University of Oxford, South Parks Road, Oxford OX1 3QU, United Kingdom[5]; Division of Biochemistry, Chiba Cancer Center Research Institute, 666-2 Nitona, Chuoh-ku, Chiba 260-8717, Japan[6]; and MGH Pathology, Harvard University, 185 Cambridge Street, Boston, Massachusetts 02114[7]

Received 8 March 2010/Returned for modification 17 April 2010/Accepted 23 October 2010

The Polycomb group of proteins forms at least two distinct complexes designated the Polycomb repressive complex-1 (PRC1) and PRC2. These complexes cooperate to mediate transcriptional repression of their target genes, including the *Hox* gene cluster and the *Cdkn2a* genes. Mammalian Polycomb-like gene Pcl2/Mtf2 is expressed as four different isoforms, and the longest one contains a Tudor domain and two plant homeodomain (PHD) fingers. Pcl2 forms a complex with PRC2 and binds to *Hox* genes in a PRC2-dependent manner. We show that Pcl2 is a functional component of PRC2 and is required for PRC2-mediated *Hox* repression. Pcl2, however, exhibits a profound synergistic effect on PRC1-mediated *Hox* repression, which is not accompanied by major alterations in the local trimethylation of histone H3 at lysine 27 (H3K27me3) or PRC1 deposition. Pcl2 therefore functions in collaboration with both PRC2 and PRC1 to repress *Hox* gene expression during axial development. Paradoxically, in embryonic fibroblasts, Pcl2 is shown to activate the expression of *Cdkn2a* and promote cellular senescence, presumably by suppressing the catalytic activity of PRC2 locally. Taken together, we show that Pcl2 differentially regulates Polycomb-mediated repression of *Hox* and *Cdkn2a* genes. We therefore propose a novel role for Pcl2 to modify functional engagement of PRC2 and PRC1, which could be modulated by sensing cellular circumstances.

The Polycomb group (PcG) was first identified in *Drosophila melanogaster* as a gene cluster necessary for the maintenance of segmental identity (50, 53). The PcG proteins are required for the epigenetic repression of a number of developmental regulatory genes, including homeotic genes. They do so by forming at least two distinct multimeric protein complexes at their target loci, known as Polycomb repressive complex-1 (PRC1) and PRC2 (11, 13, 46, 57).

In *Drosophila*, the core PRC1 is formed by four proteins, Polycomb (Pc), Polyhomeotic (Ph), Posterior sex combs (Psc), and dRing (Sex comb extra; Sce), which inhibit the chromatin remodeling activity of SWI/SNF complexes (20, 35). Mammalian orthologs form functionally similar complexes (40). PRC1 has been shown to act as an E3 component for ubiquitination of histone H2A at lysine 119 (uH2A) via Ring1B and Ring1A catalytic subunits (9, 14, 62). In addition, regulation of higher-order chromatin structure is a recently identified function mediated by PRC1 (19). The core of the mammalian PRC2 is composed of three evolutionarily conserved proteins, Eed, an ortholog of extra sex combs [Esc]), Ezh2, an ortholog of enhancer of zeste [E(z)], and Suz12, which mediates trimethylation of histone H3 at lysine 27 by the Ezh2 component (11, 13, 46, 48, 51, 60). Although both PRC1 and PRC2 are required to maintain *Hox* repression and share target loci in both vertebrates and invertebrates, these complexes do not associate with each other in most cell types. A plausible model for Polycomb silencing is through the engagement of PRC1 with the target via its interaction with H3K27me3 mediated by the chromodomain of Pc or its mammalian counterparts (11, 62). However, recent genome-wide analysis of PRC1 and PRC2 occupancy revealed that PRC1 binding demarcated a portion of the PRC2 targets (37), implying that functional engagement of PRC1 and PRC2 is not constitutive but, instead, is regulated by undefined intrinsic and/or extrinsic signals.

The *polycomblike* (*Pcl*) gene was initially isolated as a PcG gene during a *Pc* mutation modifier screen in *D. melanogaster* and then identified in several studies as an enhancer

* Corresponding author. Mailing address: RIKEN Research Center for Allergy and Immunology, 1-7-22 Suehiro, Tsurumi-ku, Yokohama 230-0045, Japan. Phone: 81 45 503 9689. Fax: 81 45 503 9688. E-mail: koseki@rcai.riken.jp.

† K.-I.I. and D.Y. contributed equally to this work.

▽ Published ahead of print on 8 November 2010.

TABLE 1. Antibodies used in this study

Specificity	Species	Antibody type	Source or reference	Catalog or clone no.
Pcl2	Mouse	Monoclonal	This paper	3A9
Pcl2	Rabbit	Antiserum	This paper	
Rnf2	Mouse	Monoclonal	5	Clone 3
Phc2	Mouse	Monoclonal	28	4G9
Mel18	Goat	Antiserum	Santa Cruz (Santa Cruz, CA)	C-20
Mel18	Rabbit	Antiserum	Santa Cruz (Santa Cruz, CA)	H-115
Eed	Mouse	Monoclonal	23	M26
Ezh2	Mouse	Monoclonal	23	M10
Ezh2	Rabbit	Monoclonal	Upstate (Lake Placid, NY)	07-400
Suz12	Rabbit	Antiserum	Upstate (Lake Placid, NY)	07-379
Histone H3K27me3	Rabbit	Antiserum	Upstate (Lake Placid, NY)	07-449
Histone H3K4me3	Rabbit	Antiserum	Upstate (Lake Placid, NY)	07-473
Histone H2Aub1	Mouse	Monoclonal	Upstate (Lake Placid, NY,)	E6C5
FLAG	Mouse	Monoclonal	Sigma-Aldrich (St. Louis, MO)	F-3165
Myc	Mouse	Monoclonal	Upstate (Lake Placid, NY)	4A6
γ-Tubulin	Rabbit	Antiserum	Sigma-Aldrich (St. Louis, MO)	T3320
$p19^{ARF}$	Rabbit	Antiserum	Abcam (Cambridge, UK)	R562
$p16^{ink4a}$	Rat	Monoclonal	NeoMarkers (Fremont, CA)	16P04

for *Esc* mutations (17, 33). *Pcl* mutant phenotypes are similar to those of *Pc* mutants, and interactions between mutant *Pcl* and *Pc* or *Esc* synergistically enhance the respective phenotypes in a dose-dependent manner. The Pcl protein has a Tudor domain and two tandem plant homeodomain (PHD) fingers (43, 49, 64). Pcl has been shown to be a part of two distinct protein complexes, PRC2 and a thus far uncharacterized complex, which appear at *Drosophila* embryonic and larval stages, respectively (47, 56, 61). In *Drosophil*a embryos, Pcl forms complexes with PRC2 and maximizes its catalytic activity at Polycomb target genes (47). In the larval stage, although Pcl does not form complexes with PRC2, it mediates pleiohomeotic-dependent PRC2 target binding (56). These findings imply that Pcl plays at least two distinct roles in regulating the expression of Polycomb targets by interacting with different protein complexes and suggest that these interactions depend on the developmental stage or cell type. The picture may be even more complex because functional interactions of Pcl could potentially extend to PRC1. In addition, Pcl has been shown to display extensive colocalization with Pc and Polyhomeotic (Ph) proteins on the polytene chromosomes (43), and genetic interactions between *Pcl* and *Pc* have also been demonstrated (33). These observations suggest that Pcl may have multiple regulatory functions in mediating Polycomb repression.

Three homologs of the *Drosophila Pcl* gene have been identified in vertebrates, frogs, chickens, and mammals and are named, *Pcl1* (also *Phf1* or *tctex3*), *Pcl2*/*Mtf2* (also *M96*; here, designated *Pcl2*) and *Pcl3* (also *Phf19*) (12, 27, 32, 36, 64, 66). Overexpression studies using *Xenopus* and chicken embryos demonstrated that Pcl1 and/or Pcl2 mediates the repression of developmental regulatory genes such as *En-2*, *Krox20*, *Hoxb9*, and *Shh* (36, 64, 66). Murine and human orthologs of these genes have been shown to be the targets of PRC1 and PRC2 as revealed by genome-wide chromatin immunoprecipitation (ChIP) assays (8, 38). These findings imply that vertebrate as well as *Drosophila* Pcl family proteins may be part of the PcG complex. In support of this idea, hPHF1 was copurified with a subset of PRC2 and was shown to enhance the catalytic activity of PRC2 in a human cell line (10, 55). Unexpectedly, however, hPHF1 was also found to form complexes with proteins involved in the DNA damage response (25). Despite these recent advances, the molecular basis underlying the multiple functions of Pcl family proteins is not well understood. Although the biochemical properties of hPHF1 have been elucidated, a genetic approach using loss-of-function mutants of the mammalian *Pcl* family is still needed to clarify the genetic cascades involving the Pcl orthologs. A study using a *Pcl2* gene trap allele suggested the involvement of Pcl2 in anterior-posterior (A-P) specification of the axis (63); however, the mechanistic basis of the involvement remains unclear. To address these questions, we have combined genetic and biochemical approaches to clarify the role of Pcl2 in Polycomb-mediated repression at the *Hox* gene cluster and *Cdkn2a* genes.

MATERIALS AND METHODS

Determination of *Pcl2* gene structure. Data sets of RNA-Seq experiments performed by Motazavi et al. (45) were downloaded (http://woldlab.caltech.edu/~alim/RNAseq/). Results from two biological replicates were summed for three cell types (brain, liver, and muscle). Positions of the 15 *Pcl2* exons (*Mtf2* in the database) were identified using the BLASTN (3) program with *Mtf2* as the reference sequence (GenBank accession number NM_013827.2) and mouse chromosome 5 (NCBI version 37) (see Fig. S1A posted at http://web.rcai.riken.jp/en/paper_figs/Li_Supp_figs_rev3.pdf).

Production of anti-Pcl2 monoclonal antibody (MAb) and antiserum. A partial cDNA fragment that included the PHD fingers (amino acids [aa] 103 tp 327) of Pcl2 was isolated by yeast two-hybrid screening for Mel18-interacters and subcloned into the pGEX-4T-3 vector (Amersham Biosciences) to express a glutathione *S*-transferase (GST)-Pcl2 fusion protein. This fusion protein was used to generate hybridomas as described previously (29). Rabbit polyclonal antiserum was raised against a synthetic polypeptide corresponding to amino acids 20 to 36 of Pcl2 (RNQKTSASLNKLSLQDGC) conjugated to keyhole limpet hemocyanin. A purified IgG fraction of this antiserum was used for immunoprecipitation (IP) and immunofluorescence.

Immunoprecipitation, Western blot analyses, and gel filtration chromatography. IP and Western blot analyses were performed as described previously (28). Antibodies used in this study are listed in Table 1 (5, 23, 28). Nuclear proteins were extracted from nuclear pellets of K562 cells as described previously (15). Nuclear extracts were loaded onto Superose 6 columns (Amersham Biosciences), and 0.5-ml fractions were collected. Proteins from each fraction were concentrated by trichloroacetic acid-deoxycholate precipita-

TABLE 2. PCR primers used in this study

Primer function	Name	Primer sequence	
		Forward	Reverse
ChIP	Hoxa4	AGCTCCAGCCCTGGCTTCGC	CGTGATGGATGCTGCTAGCC
	Hoxb4	AAACCGAGTCAAGGGGTCGG	CGCGTAGCGCTGCACAGTGC
	Hoxb6	CCGCATAGCCAGACGAGTAG	CTGCCTCTGCCATTGGTCAG
	Hoxb8	TGGAGCTGGAGAAGGAGTTCCTA	CAGAAGCTATTACGAGATACTACC
	Hprt	CTCCTAAGGTTACTAAGTAG	CAAAGGCAGTTCCGGAACTC
	Ink4a	CTACAGAAGAGATGCAGGGTTC	AAGGAGAGATTTCGAGAAGGAC
	Actin	CTACACGCTAGGCGTAAAGTTG	TCTCGTGGCTAGTACCTCACTG
RT-PCR	Hoxa1	AGATGGACAATGCAAGAATG	TCAGTGGGAGGTAGTCAGAG
	Hoxb3	ACCTACTACGACAACACCGC	TGCGACGGTTCTGGAACCAG
	Hoxb4	GATCAACTCAAACTATGTCG	TGGTGTTGGGCAACTTGTGG
	Hoxb6	GTTCCTATTTCGTGAACTCC	AGCACCTTCACTCGGCTGGC
	Hoxb8	GGAGAGGAAGCTGTATGATC	GATATCTCTTGCCTCACAAC
	Hprt	ATGAGTACTTCAGGGATTTG	TGGCCTATAGGCTCATAGTG
	Arf	CTTGGTCACTGTGAGGATTCAG	CTATGCCCGTCGGTCTGGGC
	Ink4a	TCCGCTGCAGACAGACTGGCCAG	CTATGCCCGTCGGTCTGGGC
Genotyping	$Pcl2^{WT}$	GATGGTCAGATGGCTTGTTT	AGGTAGGTAAGTGGTGGTGC
	$Pcl2^{GT}$	GATGGTCAGATGGCTTGTTT	CAAGGCGATTAAGTTGGGTAACG
	$Pcl2^{\Delta}$	GGAACTCACTCTGTAGACCCTT	CAATGCTGGGTAGGCTGA

tion. Equal amounts of each sample were run on SDS-PAGE gels and subjected to Western blot analysis.

Generation of *Pcl2* mutant mice and ES cells. The gene-trapped embryonic stem (ES) cell line for the *Pcl2* locus (M016A06) was obtained from the European Mouse Mutant Archive (24). The endogenous *Pcl2* locus was disrupted by the insertion of a retroviral U3 β-galactosidase–Neo^r fusion gene (β-geo) gene trap vector. Its insertion into exon 4 results in disruption of the *Pcl2* open reading frame (ORF) (see Fig. S2 posted at http://web.rcai.riken.jp/en/paper_figs/Li_Supp_figs_rev3.pdf).

To generate deletion mutant mice, *Pcl2* homology arms, a 3.4-kb XbaI fragment that lies at the 5′ end of the exon 4 and a 2.4-kb KpnI/SalI fragment encompassing part of exon 5, were first introduced into the pPNT-loxP-Neo vector, in which the neomycin resistance gene (Neo^r) cassette was placed between two *loxP* sites (see Fig. S3 posted at the URL mentioned above). Homologous recombinants and germ line chimeras were isolated as described previously (1) (see Fig. S3B posted at the URL mentioned above). Heterozygous mutants were bred with CAG-Cre transgenic mice to delete the Neo^r cassette (54). $Pcl2^{+/\Delta}$ mice were backcrossed six times onto a C57BL/6 background. $Pcl2^{+/\Delta}$ mice were crossed with $Phc2^{+/-}$, $Mel18^{+/-}$, and $Suz12^{+/-}$ mice to generate compound mutants. All animal experiments were carried out according to the in-house guidelines for the care and use of laboratory animals of the RIKEN, Yokohama Institute, Japan.

Homozygous mutant ES cells were derived from respective mutant embryos as described previously (14). Primer pairs used for genotyping of these mutant alleles are listed in Table 2.

ChIP analysis. ChIP analysis was performed as described previously (18, 29). The primers used in this study are listed in Table 2.

ChIP-chip and ChIP-seq analyses. We used Agilent Mouse Promoter ChIP-on-Chip Set 244K with chromatin immunoprecipitation (ChIP-chip) using antibodies against H3K27me3, Ring1B, or Pcl2. We used probes showing significant intensities above background ($P < 10^{-7}$, Student's *t* test) and located from −4 kb to +4 kb of the transcription start site (TSS) of mouse genes. Methylated, ubiquitinated, or Ring1B- or Pcl2-binding positions were defined where the signal intensity of ChIP was 4 times (H3K27me3 and Pcl2) or 10 times (Ring1B) greater than that of input and when the statistical significance between the signals was less than 10^{-3}. To reduce noise in these assays, we removed detected probes that did not have significantly strong signals from input around the 500-bp region flanking their respective positions. ChIP followed by high-throughput sequencing (ChIP-seq) analysis was performed as described previously (37). Since this study is aimed to specifically elucidate the role of Pcl2 at the *Hox* and *Cdkn2a* genes, whole data sets of these analyses will be published elsewhere.

Skeletal, *in situ* RNA, and real-time PCR analyses. Skeletal preparations were made from perinatal mice, and cleared skeletons were analyzed under a stereomicroscope as described previously (1). *In situ* hybridization of tissue sections was performed as described previously (1). RNA extraction from ES cells, reverse transcription, and PCRs were performed as described previously (21). The expression of *Hox* and *Tbx3* genes was quantified relative to *Hprt* expression by real-time PCR analyses using an Mx3005P multiplex quantitative PCR system (Stratagene). Primer pairs used for reverse transcription-PCR (RT-PCR) analysis are listed in Table 2.

Cell culture of primary MEFs. Mouse embryonic fibroblasts (MEFs) were prepared as described previously (31). The *Mel18*-null, *Mel18*/*ARF*, and *Mel18*/*p53* double-null MEFs were routinely maintained with Dulbecco's modified Eagle's medium (DMEM) supplemented with 20% fetal bovine serum (FBS), 1× nonessential amino acids (Invitrogen), and 1× penicillin-streptomycin (Invitrogen). In modified 3T9 assays, cells were passaged at 3-day intervals and counted after trypsinization, and the number of cells per dish was recorded. A total of 1×10^6 cells were replated in 60-mm diameter dishes every 3 days (31). In growth rate assays, cells diluted to 2×10^4 cells per 60-mm diameter dish were plated in duplicate, and thereafter individual cultures harvested each day were counted. The Pcl2 expression retrovirus was prepared using a retrovirus packaging system (PlatE), according to the manufacturer's instructions, and transduced into immortalized MEF $Pcl2^{GT/GT}$ cells.

RESULTS

Identification of *Pcl2* transcripts and their products. Using database screening (GenBank accession number NM_013827.2), we identified a *Pcl2* transcript that is predicted to encode a protein containing a Tudor domain, two PHD fingers in the N-terminal region, and a chromo-like domain structure in the C-terminal region (Fig. 1A, upper scheme). In addition, we found a shorter transcript encoding a protein (AAI00341.1) lacking the Tudor domain (Fig. 1A, lower scheme). To elucidate the origin of the *Pcl2* isoforms, we examined the promoter and exon usage at the *Pcl2* locus through data sets obtained from recent genome-wide analyses for H3K4me3 occupancy and RNA transcription (see Fig. S1A posted at http://web.rcai.riken.jp/en/paper_figs/Li_Supp_figs_rev3.pdf) (44, 45). *Pcl2* appears to have a single predominant transcription start site, where there is extensive H3K4 trimethylation. We further found that usage of the 15 *Pcl2* exons was not necessarily uniform and that exons 2, 3, 5, and 11 were differentially expressed among brain, liver, and muscle. This analysis suggests that the *Pcl2*

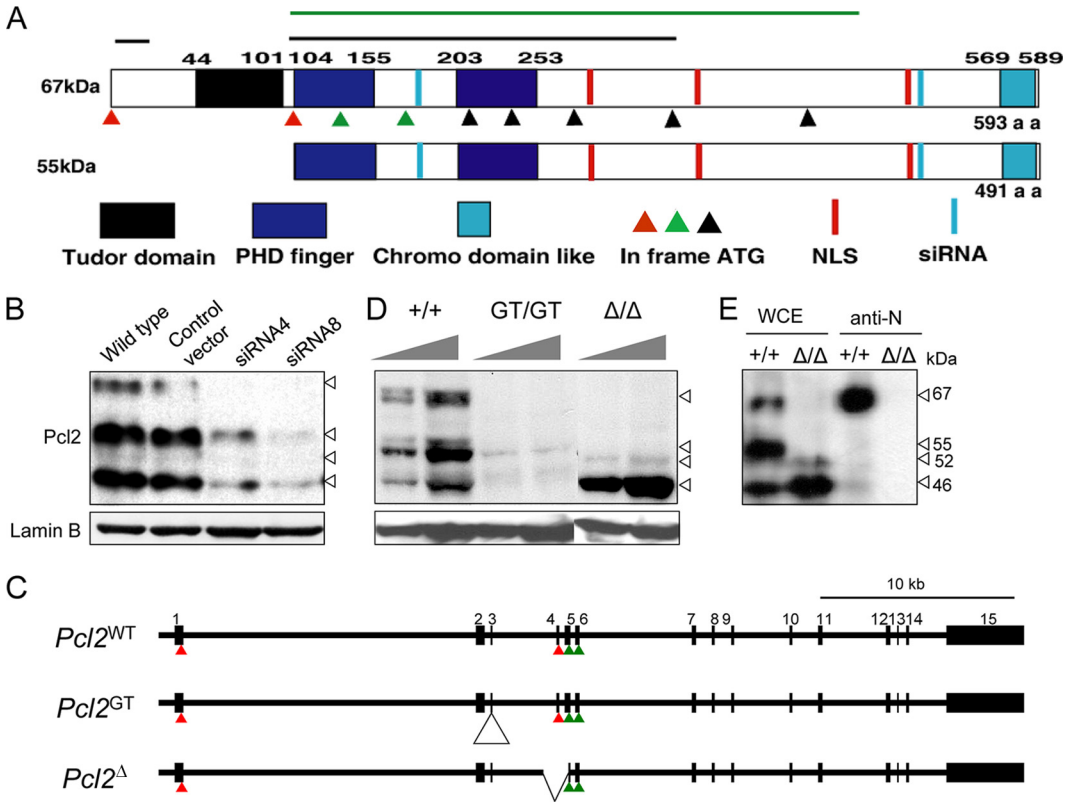

FIG. 1. Primary structure and the expression of mouse Pcl2 gene products. (A) Schematic representation of the two predicted Pcl2 isoforms. The black box corresponding to aa 44 to 101 representing the Tudor domain. The two dark blue boxes represent the PHD fingers. Three red vertical bars delineate the putative nuclear localization signals (NLS). A light blue box at aa 569 to 589 shows the chromo-like domain region at the C terminus. Positions for siRNA are demonstrated by light blue bars. The cDNA fragment isolated by two-hybrid screening for Mel18 interacting factors is shown by a green line at the top. The peptide and the fragment used to generate anti-Pcl2 antibodies are represented by two black lines. All ATG codons in the correct reading frame are indicated by colored triangles. Putative translation initiation codons for the 67- and 55-kDa isoforms are demarcated by red triangles, and those for 52- and 46-kDa isoforms are indicated by green triangles. (B) Expression of multiple Pcl2 isoforms in ES cells. The 67-, 55-, 52-, and 46-kDa bands were detected on Western blots of whole-cell lysates from wild-type ES cells using the Pcl2 MAb. The expression of *Pcl2* siRNA proportionally reduced the intensity of all four bands, whereas they were unaffected by the control siRNA. Lamin was used as a loading control. (C) Schematic representation of the genomic organization of $Pcl2^{GT}$ and $Pcl2^{\Delta}$ alleles. The $Pcl2^{GT}$ allele resulted from insertion of a gene trap vector (indicated by an open triangle) into exon 3. In the $Pcl2^{\Delta}$ allele, the genomic region encompassing the fourth intron to the middle of exon 5 is deleted. Genomic positions for putative translation initiation codons for the 67- and 55-kDa isoforms are indicated by red triangles, and those for 52- and 46-kDa isoforms are indicated by green triangles. (D) The 67-, 55-, 52-, and 46-kDa bands detected by the Pcl2 MAb were absent in $Pcl2^{GT/GT}$ ES cells, whereas only the 67- and 55-kDa bands were affected in $Pcl2^{\Delta/\Delta}$ ES cells. (E) Polyclonal antibodies against the N-terminal peptide of Pcl2 (anti-N) exclusively immunoprecipitated the 67-kDa isoform in the wild-type ES cells. WCE, whole-cell extract. The blot was probed with the Pcl2 MAb.

locus can give rise to several different transcripts, most likely due to alternative exon usage. We therefore inferred that the Pcl2 isoform lacking the Tudor domain could be produced from a transcript possessing exons 2 and 3 (see Fig. S1B posted at the URL mentioned above). In this case the nascent peptide initiating at the exon 1 start codon would prematurely terminate because of a frameshift; instead, productive translation would initiate at the start codon in exon 4, giving rise to a protein equivalent to AAI00341.1 (indicated by a green triangle in Fig. S1B posted at the URL mentioned above).

We then used Western blot analysis using a MAb produced against a GST-Pcl2 (aa 103 to 327) fusion protein to examine the expression of Pcl2 gene products. The MAb reproducibly detected strong bands of 67, 55, and 46 kDa and a much weaker 52-kDa band in whole-cell extracts of wild-type ES cells (Fig. 1B). To clarify whether these bands represent isoforms of Pcl2, we measured the effect of small interfering RNA (siRNA)-mediated knockdown of *Pcl2* in ES cells (Fig. 1A) on the appearance of the bands. Expression of two different siRNA constructs reduced the intensity of all four bands proportionally (Fig. 1B). These data indicate that *Pcl2* is expressed primarily as 67-, 55-, 52-, and 46-kDa isoforms.

To further elucidate the origin of the Pcl2 isoforms, we used two mutant alleles for *Pcl2*. Insertion of a gene-trap vector into exon 3 ($Pcl2^{GT}$) is expected to impair the expression of Pcl2 (Fig. 1C; see also Fig. S2 posted at http://web.rcai.riken.jp/en/paper_figs/Li_Supp_figs_rev3.pdf). In $Pcl2^{GT/GT}$ ES cells, we found this insertion diminished band intensities (Fig. 1D). In another allele, we deleted exon 4 and part of exon 5 by targeted mutagenesis ($Pcl2^{\Delta}$) (Fig. 1C; see also Fig. S3 posted at the URL mentioned above). This deletion resulted in the expression of truncated *Pcl2* transcripts in which exon 4 and 5 were skipped (X. Li, unpublished observations). These truncated

transcripts are predicted to encode a Pcl2 protein lacking the Tudor domain and the first PHD finger. Consistent with this prediction, the 67- and 55-kDa bands were abolished in $Pcl2^{\Delta/\Delta}$ ES cells. Therefore, the 67- and 55-kDa isoforms represent proteins with and without the Tudor domain, respectively (Fig. 1A). To validate this interpretation, we generated a polyclonal antibody against a synthetic polypeptide corresponding to part of the Pcl2 Tudor domain (aa 20 to 36). This antibody exclusively immunoprecipitated the 67-kDa band, confirming the presence of the Tudor domain in this isoform (Fig. 1E).

***Hox* repression by Pcl2.** *Hox* cluster genes are evolutionarily conserved targets for Polycomb repression during A-P specification of the axis. We thus examined axial skeletal development in $Pcl2^{GT/GT}$ and $Pcl2^{\Delta/\Delta}$ mice. Both mutant mice survived to birth; however, most of the $Pcl2^{GT/GT}$ mice died before weaning. In contrast, $Pcl2^{\Delta/\Delta}$ mice were viable and fertile. Although postnatal viabilities of the $Pcl2^{GT/GT}$ and $Pcl2^{\Delta/\Delta}$ mice were different, similar axial skeletal alterations that are characteristic of posterior transformations were observed in both mutants, as shown in a previous study (65) (Fig. 2A and B). Briefly, ectopic ribs that associated with the seventh cervical vertebra (C7) were frequently seen in $Pcl2^{GT/GT}$ and $Pcl2^{\Delta/\Delta}$ mice (indicated by arrows in Fig. 2A, frames b, c, e, f, n, and o). Consistent with this malformation, sternums were shifted anteriorly (indicated by brackets in Fig. 2A, frames b and c). The odontoid process, which is normally a characteristic of the second cervical vertebra (C2), was frequently associated with the first cervical vertebra (C1) in the mutants (indicated by red triangles in Fig. 2A, frames h to j). Axial skeletal changes indicating posterior transformations were also manifested at thoracolumbar and lumbosacral transitions of $Pcl2^{GT/GT}$ and $Pcl2^{\Delta/\Delta}$ mice (Fig. 2B). Therefore, Pcl2 proteins, particularly the 67- and/or 55-kDa isoforms, are required for A-P specifications of the axis, similar to other PcG proteins.

Next, we used *in situ* hybridization analysis to determine whether homeotic transformations in $Pcl2^{\Delta/\Delta}$ mice were accompanied by *Hox* gene derepression. The anterior boundaries of *Hoxb4*, *Hoxb6*, *Hoxb8*, and *Hoxd4* expression in the developing sclerotome were shifted cranially in $Pcl2^{\Delta/\Delta}$ embryos at 11.5 days postcoitus (dpc) (Fig. 2C). These results are consistent with homeotic transformations in the cervical and cervicothoracic boundary regions. We also found subtle but significant derepression of several *Hox* genes in $Pcl2^{\Delta/\Delta}$ ES cells (Fig. 2D). These results show that Pcl2 regulates *Hox* gene expression.

Pcl2 binds to *Hox* genes in a PRC2-dependent manner. Recent chromatin immunoprecipitation (ChIP) analyses revealed deposition of PRC2, PRC1, and H3K27me3 at the *Hox* cluster in developing embryos and ES cells. In parallel, *Drosophila* Pcl and human PHF1 were shown to be included in PRC2 in *Drosophila* and human cells, respectively (10, 47, 55, 56). Moreover, ChIP-seq studies reported significant overlap of genes bound by Pcl2 and Ezh2 in ES cells (41). These observations prompted us to hypothesize that Pcl2 mediates *Hox* repression via direct association with the *Hox* genes. By conventional ChIP assay using an anti-Pcl2 polyclonal antibody, we immunoprecipitated promoter regions of *Hoxb4*, *Hoxb6*, and *Hoxb8* from the wild-type ES cells but not from $Pcl2^{\Delta/\Delta}$ ES cells, which were used as a negative control (Fig. 3A). This result was further validated by ChIP-chip analysis using $Pcl2^{GT/GT}$ ES cells, which are reconstituted with the 67-kDa isoform of myc-tagged Pcl2. Here, an anti-myc antibody was used instead of the polyclonal antibody against the N-terminal peptide of Pcl2 (anti-N). In this experiment, too, we found considerable Pcl2 deposition around the transcription start sites (TSSs) of the *Hox* gene cluster, all of which were cooccupied by H3K27me3 and Ring1B (Fig. 3B; also D. Yamada and H. Koseki, unpublished data). Based on these results, we extended our analyses to the entire *Hoxd* cluster by ChIP-seq analysis using the anti-Pcl2 polyclonal antibody (Fig. 3C) (37). Indeed, the distribution profile of Pcl2 at the *Hoxd* cluster was similar to that of both Ezh2 and Ring1B. In particular, clear peaks that represented extensive binding of Pcl2, Ezh2, and Ring1B appeared concurrently around *Hoxd9*, *Hoxd10*, *Hoxd11*, *Hoxd12*, *Hoxd13*, and *Evx2*. Therefore, Pcl2 binds to *Hox* cluster genes, and its binding is correlated with local depositions of PRC2 and PRC1.

We went on to test whether Pcl2 expression and target binding depend on PRC2 because the expression of PRC2 components is known to be mutually dependent, and Pcl2 has already been reported as a PRC2-associated protein in mouse ES cells (21, 41, 63) (see Fig. S4 posted at http://web.rcai.riken.jp/en/paper_figs/Li_Supp_figs_rev3.pdf). In agreement with this view, we observed that the expression of Pcl2, as well as of Eed and Ezh2, was considerably decreased in $Suz12^{-/-}$ ES cells (Fig. 3D) (21). Particularly, the 67- and 55-kDa isoforms of Pcl2 were almost absent. We further used ChIP assays to confirm this result. Consistent with the reduction of Pcl2 expression in $Suz12^{-/-}$ ES cells, Pcl2 binding was almost nonexistent (Fig. 3E). It is worth noting that level of *Pcl2* transcripts was not proportionally altered in comparison to that of Pcl2 proteins in $Suz12^{-/-}$ ES cells (Fig. 3F). This suggests that Pcl2 expression is posttranscriptionally regulated in a PRC2-dependent manner. In contrast, the expression of Pcl2 and its binding to *Hox* genes were unaffected in $Ring1B^{-/-}$ ES cells (Fig. 4A and B). Moreover, the expression of PRC2 and PRC1 and their binding to *Hox* genes were not affected in $Pcl2^{\Delta/\Delta}$ ES cells (Fig. 4C and D). In summary, we conclude that Pcl2 binds to *Hox* genes in a PRC2-dependent manner.

***Hox* repression by Pcl2 involves its functional interactions with PRC2 and PRC1.** We went on to test whether *Hox* repression by Pcl2 involves its interactions with PRC2. It is well established that Polycomb components cooperate to mediate *Hox* repression via physical interactions. Indeed, *Drosophila Pcl* was isolated as an enhancer for the *extra sex combs* (*esc*) mutation (33). Therefore, we examined the interactions between *Pcl2* and *Suz12* (an essential component of PRC2) mutant alleles. Since *Suz12* homozygous mutants die around 8.5 dpc, heterozygous embryos were used. Notably, even the heterozygous mutants exhibited homeotic transformations of the axis, albeit to a lesser extent than $Pcl2^{\Delta/\Delta}$ mutants (Fig. 5A and B) (21). The skeletal phenotypes were compared between $Pcl2^{\Delta/\Delta}$ and $Pcl2^{\Delta/\Delta}$; $Suz12^{+/-}$ mice at the newborn stage, and significant differences were identified around the cervicothoracic boundary. Anterior tuberculums, which are characteristic of the C6 vertebra, were associated instead with the C5 in $Pcl2^{\Delta/\Delta}$; $Suz12^{+/-}$. The C7 vertebrae were associated with perfect ribs, which were attached to the anteriorly shifted sternum.

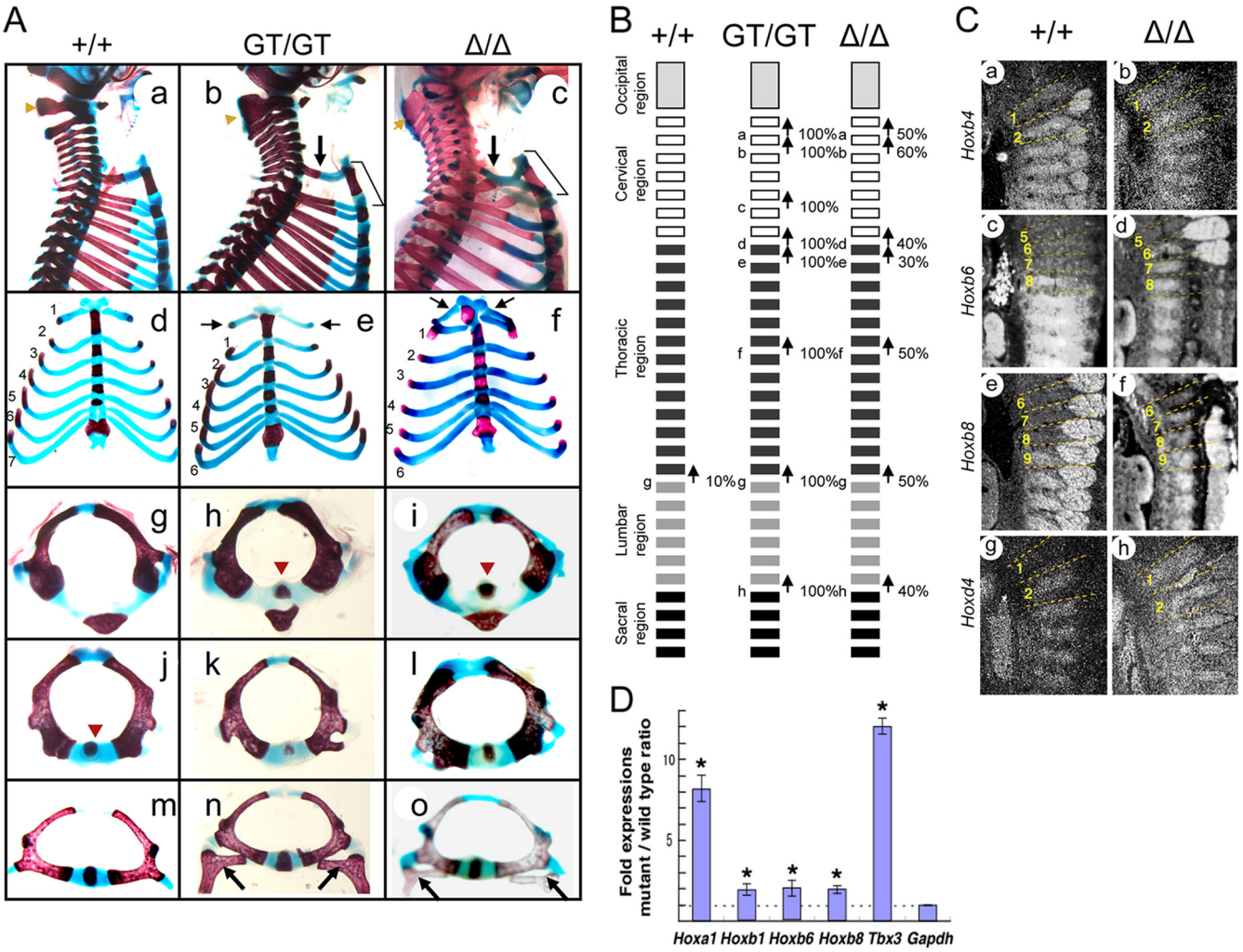

FIG. 2. Posterior transformation of the axis in *Pcl2*$^{GT/GT}$ and *Pcl2*$^{\Delta/\Delta}$ mutants. (A) Skeletal alterations in *Pcl2*$^{GT/GT}$ (GT/GT) and *Pcl2*$^{\Delta/\Delta}$ (Δ/Δ) mutants. (Frames a, b, and c) Lateral views of the upper part of the vertebral column are shown. Yellow arrowheads indicate the first cervical vertebra. The arrows and brackets in frames b and c indicate the ectopic ribs associated with C7 and the anteriorly shifted sternum, respectively. (Frames d, e, and f) Ventral views of the rib cages are shown. In frames e and f, the ectopic ribs associated with C7 are indicated by arrows. (Frames g, h, and i) Overviews of isolated C1 vertebrae. Odontoid processes fused with C1 are indicated by arrowheads in frames h and i. (Frames j, k, and l) Overviews of isolated C2 vertebrae. The odontoid process is indicated by an arrowhead in frame j. (Frames m, n, and o) Overviews of isolated C7 vertebrae. Ectopic ribs are indicated by arrows in frames n and o. (B) Schematic summary of the axial homeotic transformations in *Pcl2*$^{GT/GT}$ and *Pcl2*$^{\Delta/\Delta}$ mice. The following parameters, identified by letters on the figure, were scored, and the frequency of each alteration is indicated: C1 → C2, presence of the odontoid process on the C1 vertebra (a); C2 → C3, lack of the odontoid process from the C2 vertebra (b); C5 → C6, appearance of anterior tuberculum (c); C7 → T1, appearance of cervical ribs on C7 (d); T1 → T2, prominent spinous process on T1 (e); T7 → T8, dissociation of seventh rib from the sternum (f); T13 → L1, loss of the rib on 20th vertebra (g); lumbar vertebra 5 (L5) or L6 → sacral vertebra 1 (S1), formation of the sacroiliac joint in 25th or 26th vertebra (h). (C) Expression of *Hox* genes in 11.5-dpc wild-type and *Pcl2*$^{\Delta/\Delta}$ embryos. The expression of *Hoxb4* (a and b), *Hoxb6* (c and d), *Hoxb8* (e and f), and *Hoxd4* (g and h) is shown. Prevertebrae are numbered starting from the proatlas, and dotted lines indicate the segment boundaries. (D) Derepression of *Hox* genes in *Pcl2*$^{\Delta/\Delta}$ ES cells. *Hoxa1*, *Hoxb4*, *Hoxb6*, *Hoxb8*, and *Tbx3* were derepressed in *Pcl2*$^{\Delta/\Delta}$ ES cells compared to the wild-type controls by real-time PCR. Fold expression of respective genes in *Pcl2*$^{\Delta/\Delta}$ ES cells compared to that of the wild type is shown by bars. Statistically significant differences are indicated by asterisks.

A prominent spinous process, which appeared on thoracic vertebra 2 (T2) in the wild-type, *Suz12*$^{+/-}$, and *Pcl2*$^{\Delta/\Delta}$ pups, was frequently associated with the T1 in *Pcl2*$^{\Delta/\Delta}$; *Suz12*$^{+/-}$ mutants. In summary, heterozygous loss of *Suz12* synergistically enhanced the homeotic transformations of *Pcl2* single mutants. Taken together, we conclude that *Hox* repression by Pcl2 involves its interaction with PRC2. Since Pcl and PHF1 are known to enhance the catalytic activity of PRC2, we inferred that Pcl2 contributes to *Hox* repression by regulating PRC2 activity. We did not, however, observe extensive changes in global and local levels of H3K27me3 in *Pcl2*$^{\Delta/\Delta}$ ES cells (Fig. 4C and D). Supporting this observation, binding of Ring1B to *Hox* genes was not changed despite *Hox* derepression in ES cells. As the molecular mechanisms that underlie Pcl2-dependent regulation of PRC2 are still unclear, we speculated that Pcl2-mediated *Hox* repression might involve PRC1.

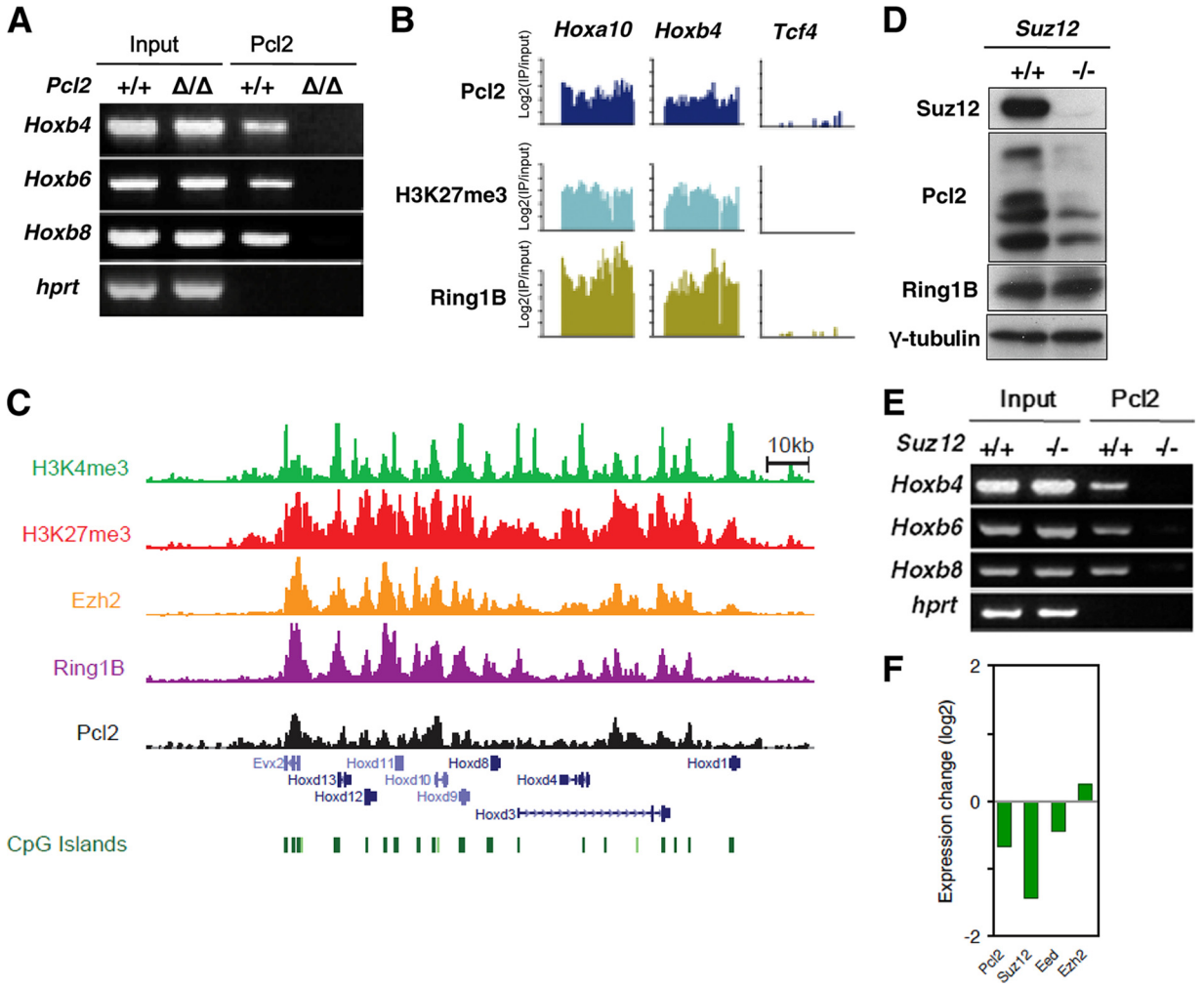

FIG. 3. PRC2-dependent binding of Pcl2 to *Hox* genes. (A) Pcl2 association at *Hox* promoter regions revealed by conventional ChIP assay using anti-N polyclonal in $Pcl2^{+/+}$ (+/+) and $Pcl2^{\Delta/\Delta}$ (Δ/Δ) ES cells. For the input, genomic DNA extracted from the original whole-cell lysate equivalent to 1/40 of the volume used for the ChIP analysis was subjected to PCR; the *hprt* gene was used as a negative control. (B) The distribution of Pcl2, H3K27me3, and Ring1B at the promoter regions of the genes in ES cells. Agilent mouse promoter ChIP-on-Chip Sets 244K were used for *Hoxa10*, *Hoxb4*, and *Tcf4* promoter region analysis. (C) ChIP-seq binding patterns for *Evx2* and *Hoxd* loci are shown for H3K4me3, H3K27me3, Ezh2, Ring1B, and Pcl2 in ES cells. CpG islands are shown as green bars (below). (D) Impact of Suz12 deficiency on the expression of Pcl2. The expression of Suz12, Pcl2, Rnf2, and γ-tubulin in $Suz12^{+/+}$ (+/+) and $Suz12^{-/-}$ (−/−) ES cells as revealed by Western blotting. (E) Pcl2 association at *Hox* promoter regions in $Suz12^{+/+}$ and $Suz12^{-/-}$ ES cells. For the input, genomic DNA extracted from the original whole-cell lysate equivalent to 1/40 of the volume used for the ChIP analysis was subjected to PCR; the *hprt* gene was used as a negative control. (F) Expression changes of *Pcl2*, *Suz12*, *Eed*, and *Ezh2* in $Suz12^{-/-}$ ES cells. Expression changes of *Pcl2*, *Suz12*, *Eed*, and *Ezh2* in $Suz12^{-/-}$ ES cells were revealed by microarray analysis using Affymetrix Mouse 430.2. Detected signals were normalized using a quantile normalization method, and only signals having significant intensity from background were counted. The average signal intensity of respective genes in $Suz12^{-/-}$ and wild-type ES cells was calculated, and the log ratios of $Suz12^{-/-}$ against wild type are shown by bars.

We thus examined whether the *Pcl2* mutation functionally interacts with mutations in genes encoding PRC1 components since previous reports have shown that compound mutants of PRC1 genes have a more severe phenotype than single mutants, suggesting the importance of such cooperativity (2, 6). We therefore compared the axial skeletal abnormalities in $Pcl2^{\Delta/\Delta}$; $Mel18^{-/-}$ and $Pcl2^{\Delta/\Delta}$; $Mel18^{+/+}$ mice. Notably, no viable $Pcl2^{\Delta/\Delta}$; $Mel18^{-/-}$ mice were seen at the perinatal stage, whereas the respective single homozygotes ($Pcl2^{\Delta/\Delta}$; $Mel18^{+/+}$ and $Pcl2^{+/+}$; $Mel18^{-/-}$) survived. Because of this, the skeletal phenotypes were examined at 16.5 dpc. $Mel18^{-/-}$ fetuses had phenotypes that were nearly identical to those in the $Pcl2^{\Delta/\Delta}$ fetuses, as reported previously (1). The $Pcl2^{\Delta/\Delta}$; $Mel18^{-/-}$ double mutants showed more stringent transformations than either of the single mutants (Fig. 5C and D). Occipital bones were segmented, resulting in the formation of an ectopic arch. The C1 vertebrae were identical to the wild-type C2, and perfect ribs bridged an anteriorly shifted sternum and the C7. Interestingly, a hole reproducibly appeared at the central region of the scapula of $Pcl2^{\Delta/\Delta}$; $Mel18^{-/-}$ mice, which was not seen in either of the single mutants. A similar synthetic defect in the scapula has been reported in $Mel18^{-/-}$; $Phc2^{-/-}$ and $Mel18^{-/-}$; $Bmi1^{+/-}$ mice due to the combined effects of the respective mutations (2, 28). Taken together, the genetic in-

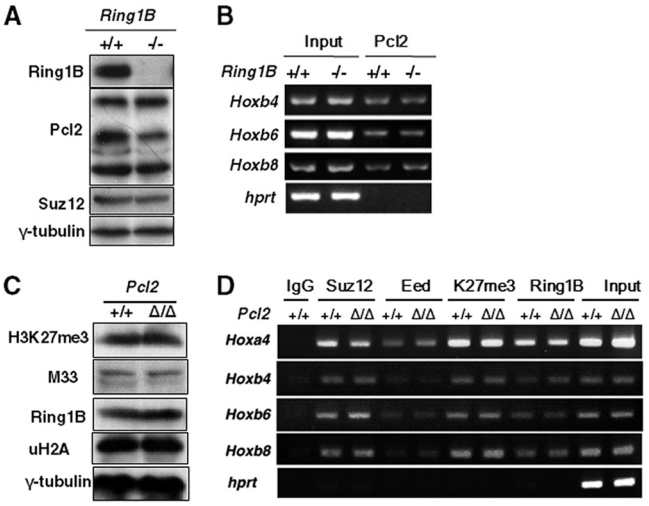

FIG. 4. The expression and target binding of Ring1B and Pcl2 are regulated in a mutually independent manner in ES cells. (A) Pcl2 and Suz12 are expressed in a Ring1B-independent manner. The expression of Ring1B, Pcl2, and Suz12 in *Ring1B*$^{+/+}$ and *Ring1B*$^{-/-}$ ES cells is shown. γ-Tubulin was used as a dose control. (B) Pcl2 binds to *Hox* promoters in a Ring1B-independent manner. Pcl2 association to the *Hox* promoter regions in *Ring1B*$^{+/+}$ and *Ring1B*$^{-/-}$ ES cells is shown. The *hprt* gene was used as a negative control. (C) Global levels of H3K27 trimethylation (H3K27me3), M33, Ring1B, and H2A monoubiquitinylation (uH2A) were not significantly altered in *Pcl2*$^{\Delta/\Delta}$ ES cells (Δ/Δ) compared to levels in the wild type (+/+). γ-Tubulin was used as a dose control. (D) Binding of Suz12, Eed, H3K27me3, and Ring1B at *Hox* promoter regions was not significantly changed in *Pcl2*$^{\Delta/\Delta}$ ES cells (Δ/Δ). IgG and *hprt* genes were used as negative controls.

teractions between *Pcl2* and *Mel18* mutations synergistically enhanced skeletal abnormalities of the respective mutants and influenced the survival of late-gestation fetuses. To further clarify whether interactions between *Pcl2* and *Mel18* involve PRC1, we extended our genetic studies to Phc2, which is another PRC1 component and is known to physically and genetically interact with Mel18 (28). The *Pcl2*$^{\Delta/\Delta}$; *Phc2*$^{-/-}$ fetuses exhibited skeletal phenotypes and late-gestational lethality very similar to the patterns seen in not only *Pcl2*$^{\Delta/\Delta}$; *Mel18*$^{-/-}$ but also *Mel18*$^{-/-}$; *Phc2*$^{-/-}$ and *Phc1*$^{+/-}$; *Phc2*$^{-/-}$ mutants (Fig. 5C and D). These observations indicate a role for Pcl2 in reinforcing *Hox* repression that is mediated by PRC1. The cooccupancy of *Hox* genes by Pcl2 together with PRC2 and PRC1 suggests that Pcl2 positively regulates PRC2 and PRC1 to repress *Hox* genes during A-P specification of the axis.

***Cdkn2a* activation by Pcl2 in MEFs involves suppression of PRC2.** We went on to examine the functional implication of Pcl2 to mediate Polycomb repression in other cellular contexts. Senescence is a fundamental cellular program that is activated under various forms of stress and acts to prevent further cell proliferation. When a population of cells is propagated in culture, they are exposed to various extrinsic and intrinsic stresses, and the cell population gradually stops dividing. Two definitive tumor suppressor pathways, ARF/MDM2/p53 and p16^{INK4a}/Rb, have been shown to play critical roles in the induction of cellular senescence (59). Central mediators for cellular senescence, p19^{arf} and p16^{Ink4a}, are encoded by the *Cdkn2a* locus, which is known as an essential target of PRC1 (30). PRC1 represses p19^{arf} and p16^{Ink4a} in embryonic fibroblasts (MEFs) and thus protects MEFs to some extent from stress-induced premature senescence. This PRC1-dependent regulation of *Cdkn2a* has also been shown to be active in various stem and progenitor cells.

We first examined the binding of Pcl2 to the *Cdkn2a* locus by ChIP-seq analysis and found considerable Pcl2 deposition together with Ezh2, H3K27me3, and Ring1B in ES cells (Fig. 6A). To test the role of Pcl2 in the regulation of p19^{arf} and p16^{Ink4a} expression, we generated MEFs from *Pcl2*$^{\Delta/\Delta}$ and wild-type littermates and compared progression of cellular senescence by a 3T9 assay (Fig. 6B). To our surprise, growth of *Pcl2*$^{\Delta/\Delta}$ MEFs was similar to that of wild-type MEFs until passage 10, but then the cells failed to stop dividing and continued exponential growth over 50 passages while *Phc2*$^{-/-}$ MEFs prematurely senesced. We further found that *Pcl2*$^{GT/GT}$ MEFs similarly bypassed senescence (Fig. 6C). To confirm that this effect is directly due to Pcl2 loss, we expressed Pcl2 in immortalized *Pcl2*$^{GT/GT}$ MEFs by retroviral transduction. Ectopic expression of Pcl2 indeed induced cellular senescence in immortalized *Pcl2*$^{GT/GT}$ MEFs (Fig. 6D). Consistent with these phenotypes, *Pcl2*$^{\Delta/\Delta}$ MEFs did not exhibit morphological features characteristic of senescent MEFs at passage 12 (Fig. 6E). We went on to investigate the expression of p19^{arf} and p16^{Ink4a} in *Pcl2*$^{\Delta/\Delta}$ MEFs and observed their strong repression at passage 10 (Fig. 6F). This was accompanied by a reduction of *p19*^{arf} and *p16*^{Ink4a} transcripts (Fig. 6G). Therefore, these results suggest that *Pcl2*$^{\Delta/\Delta}$ MEFs fail to undergo cellular senescence.

We next tested the functional involvement of *Cdkn2a* repression in terminating cellular senescence. To this end, we expressed p19^{arf} or p16^{Ink4a} in *Pcl2*$^{\Delta/\Delta}$ MEFs by retroviral transduction. Proliferation of *Pcl2*$^{\Delta/\Delta}$ MEFs was clearly inhibited by either p19^{arf} or p16^{Ink4a} (Fig. 6H), thus suggesting that Pcl2 promotes cellular senescence by activating the expression of *Cdkn2a* genes in MEFs. To further test this hypothesis, we overexpressed Pcl2 in MEFs. We generated a transgenic mouse, in which expression of the 67-kDa isoform of Pcl2 could be induced by tamoxifen-dependent activation of ERT2-Cre (Fig. 7A). Proliferation of these MEFs was impaired by tamoxifen treatment (Fig. 7B), and the mitotic arrest was accompanied by activation of p19^{arf} (Fig. 7C). Therefore, we showed that Pcl2 plays a role as an activator of *Cdkn2a* expression, whereas PRC1 functions as a repressor in MEFs.

We went on to test whether this positive effect of Pcl2 on *Cdkn2a* transcription involved regulation of the catalytic activity of PRC2. We performed ChIP analysis to test H3K27me3 occupancy at the *p16*^{Ink4a} promoter region in *Pcl2*$^{GT/GT}$ MEFs (Fig. 8A and B). Local H3K27me3 levels at this promoter were significantly increased in *Pcl2*$^{GT/GT}$ MEFs compared to levels the wild-type cells. Consistent with the transcriptional status of *p16*^{Ink4a}, we also found decrease H3K4me3 in *Pcl2*$^{GT/GT}$ MEFs. Pcl2 therefore activates *Cdkn2a* expression, presumably by suppressing local catalytic activity of PRC2.

In addition, we examined whether Pcl2-dependent regulation of *Cdkn2a* involves PRC1. We generated *Pcl2* and *Phc2* double mutant MEFs and compared the level of cellular senescence to that observed in the single mutants (Fig. 6B). Notably, *Pcl2*$^{\Delta/\Delta}$; *Phc2*$^{-/-}$ MEFs, as well as *Phc2*$^{-/-}$ MEFs,

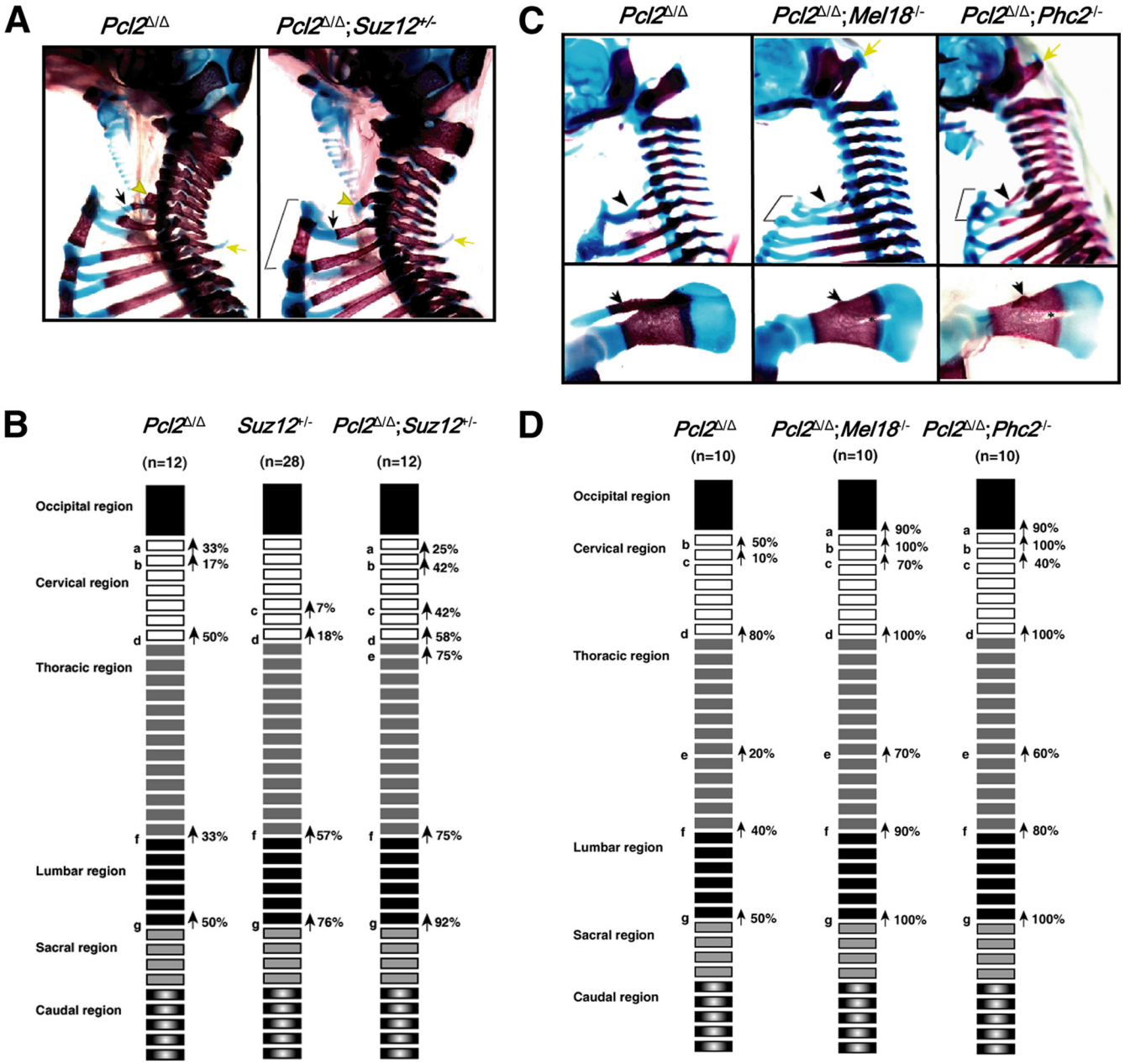

FIG. 5. Synergistic activity of Pcl2 with PRC2 and PRC1 components during A-P specification of the axis. (A) Lateral views of the upper part of the vertebral column in *Pcl2*$^{\Delta/\Delta}$ and *Pcl2*$^{\Delta/\Delta}$; *Suz12*$^{+/-}$ newborn mice. Genotypes of *Pcl2* and *Suz12* loci are indicated at the top. Anterior tubercles, ectopic ribs, and prominent spinous processes are indicated by yellow arrowheads, black arrows, and yellow arrows, respectively. A bracket in *Pcl2*$^{\Delta/\Delta}$; *Suz12*$^{+/-}$ indicates the cranially shifted sternum. (B) Schematic representation of the frequency of the axial homeotic transformations in respective mutants. The following parameters, identified by letters on the figure, were scored, and the frequency of each alteration is indicated: C1 → C2, presence of the odontoid process on the C1 vertebra (a); C2 → C3, lack of the odontoid process from the C2 vertebra (b); C5 → C6, appearance of the anterior tubercle of the transverse process on the C5 (c); C7 → T1, appearance of cervical ribs on C7 (d); T1 → T2, prominent spinous process on T1 (e); T13 → L1, loss of the rib on 20th vertebra (f); L5 or L6 → S1, formation of the sacroiliac joint in the 25th or 26th vertebra (g). (C) Skeletal alterations seen in *Pcl2*$^{\Delta/\Delta}$, *Pcl2*$^{\Delta/\Delta}$; *Mel18*$^{-/-}$, and *Pcl2*$^{\Delta/\Delta}$; *Phc2*$^{-/-}$ mice. Only the mutant *Pcl2*, *Mel18*, and *Phc2* alleles are depicted. (Upper panels show lateral views of the upper part of the vertebral column. Arrowheads indicate ectopic ribs associated with C7. For *Pcl2*$^{\Delta/\Delta}$; *Mel18*$^{-/-}$ and *Pcl2*$^{\Delta/\Delta}$; *Phc2*$^{-/-}$ mice, yellow arrows and brackets indicate ectopic arches of the occipital bone and cranially shifted sternum, respectively. Lower panels show overviews of the scapula. Acromion are indicated by arrows, which are rudimentary in the compound mutants. Holes (asterisks) were generated in the center of blades in *Pcl2*$^{\Delta/\Delta}$; *Mel18*$^{-/-}$ and *Pcl2*$^{\Delta/\Delta}$; *Phc2*$^{-/-}$ mice. (D) Schematic representation of the frequency of the axial homeotic transformations in respective mutants. The following parameters, identified by letters on the figure, were scored, and the frequency of each alteration is indicated: supraoccipital bone → C1, appearance of ectopic bones seen in the craniodorsal region of the C1 vertebra or ectopic arch of the occipital bones (a); C1 → C2, presence of the odontoid process on the C1 vertebra (b); C2 → C3, lack of the odontoid process from the C2 vertebra (c); C7 → T1, appearance of cervical ribs on C7 (d); T7 → T8, dissociation of seventh rib from the sternum (e); T13 → L1, loss of the rib on the 20th vertebra (f); L5 or L6 → S1, formation of the sacroiliac joint in 25th or 26th vertebra (g).

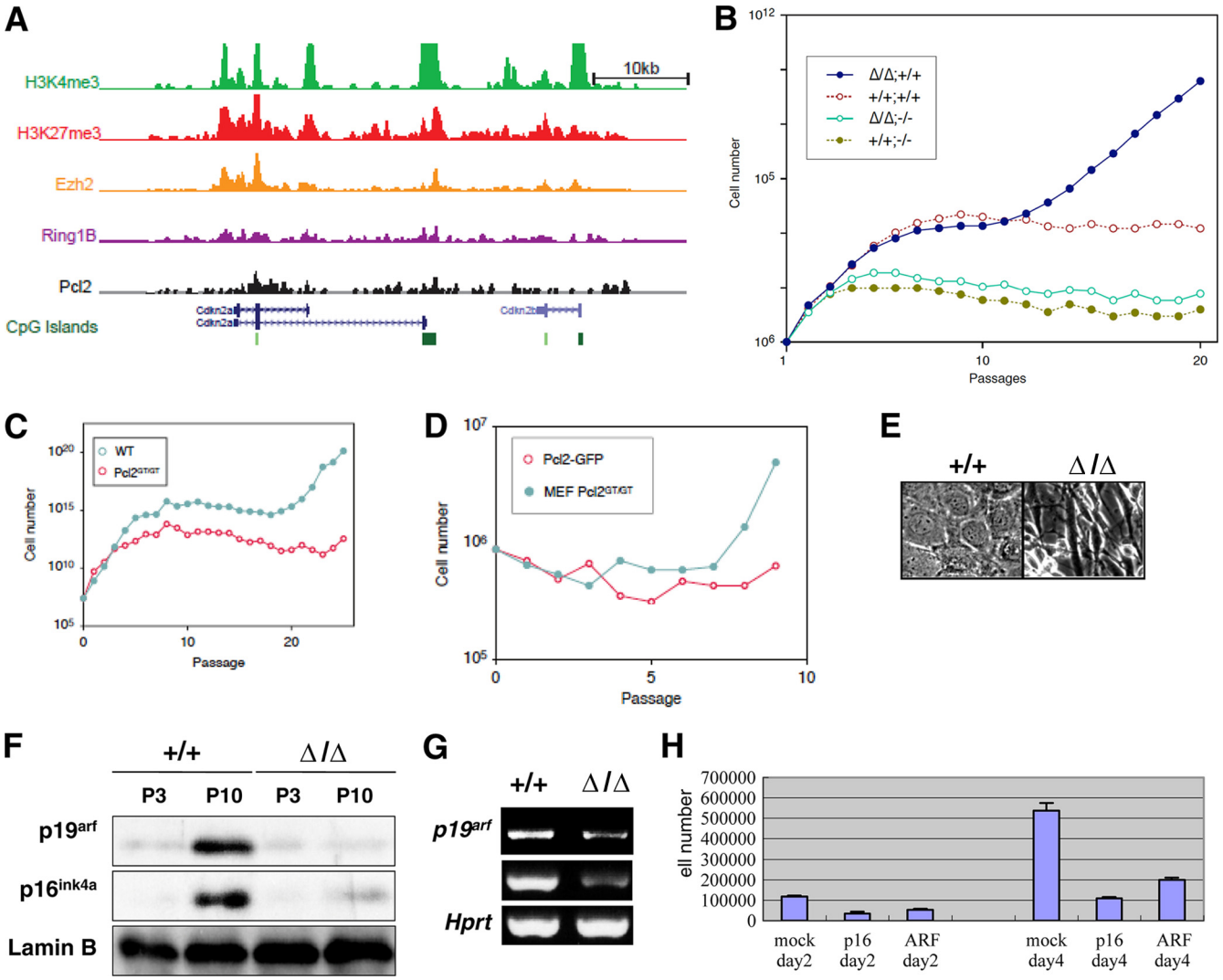

FIG. 6. The role of Pcl2 in replicative senescence. (A) ChIP-seq binding patterns at *Cdkn2a* and *Cdkn2b* loci are shown for H3K4me3, H3K27me3, Ezh2, Ring1B, and Pcl2 in ES cells. CpG islands are shown as green bars (below) (B) Termination of replicative senescence in $Pcl2^{\Delta/\Delta}$ MEFs as revealed by a modified 3T9 assay. Levels of replicative senescence were compared among the wild-type (+/+; +/+), $Pcl2^{\Delta/\Delta}$ (Δ/Δ; +/+), $Phc2^{-/-}$ (+/+; −/−) and $Pcl2^{\Delta/\Delta}$; $Phc2^{-/-}$ (Δ/Δ; −/−) cells. (C) The role of Pcl2 in replicative senescence. Termination of replicative senescence in $Pcl2^{GT/GT}$ MEFs as revealed by a modified 3T9 assay. Levels of replicative senescence were compared between the wild-type (+/+; +/+) and $Pcl2^{GT/GT}$ MEFs. (D) Overexpression of Pcl2 induced senescence in $Pcl2^{GT/GT}$ MEFs. (E) Morphology of wild-type (+/+) and $Pcl2^{\Delta/\Delta}$ (Δ/Δ) MEFs at passage 12. Light microscopic views are shown. (F) Decreased expression of $p19^{arf}$ and $p16^{ink4a}$ in $Pcl2^{\Delta/\Delta}$ (Δ/Δ) MEFs at passage 10 in comparison with that of the wild type (+/+). The expression of lamin B was examined as a dose control. (G) Quantitative analysis of $p19^{arf}$ and $p16^{ink4a}$ transcripts in $Pcl2^{\Delta/\Delta}$ (Δ/Δ) MEFs at passage 10. Note the concomitant reduction of these transcripts in $Pcl2^{\Delta/\Delta}$ MEFs in comparison with wild type (+/+). (H) *Cdkn2a* repression is involved in inhibiting cellular senescence in $Pcl2^{\Delta/\Delta}$ MEFs. Overexpression of either $p19^{arf}$ or $p16^{Ink4a}$ in $Pcl2^{\Delta/\Delta}$ MEFs considerably inhibited their proliferation. The total cells were counted on day 2 and day 4 after retroviral transduction.

stopped replicating at passage 5. Therefore, the *Pcl2*-deficient phenotype was strongly suppressed by loss of *Phc2*, which implies that Pcl2 functions require PRC1 in regulation of cellular senescence. Consistently, we found a considerable quantity of Ring1B retained at the $p16^{Ink4a}$ promoter in $Pcl2^{GT/GT}$ MEFs although its local level was significantly decreased compared to that of the wild type (Fig. 8A and B). Pcl2 thus profoundly modulates functional engagement of PRC2 and PRC1 to maintain proper expression of *Cdkn2a* under replicative stress.

DISCUSSION

In this study, we have investigated the role of Pcl2 at two canonical Polycomb targets, the *Hox* cluster and *Cdkn2a* genes, by combining genetic and biochemical approaches. We have first identified Pcl2 gene products and their functions in *Hox* repression during A-P specification by using two mutant alleles. The expression of Pcl2 and its binding to *Hox* genes were shown to depend on its physical association with PRC2. Interactions of mutant *Pcl2* with *Suz12* indicated the requirement of

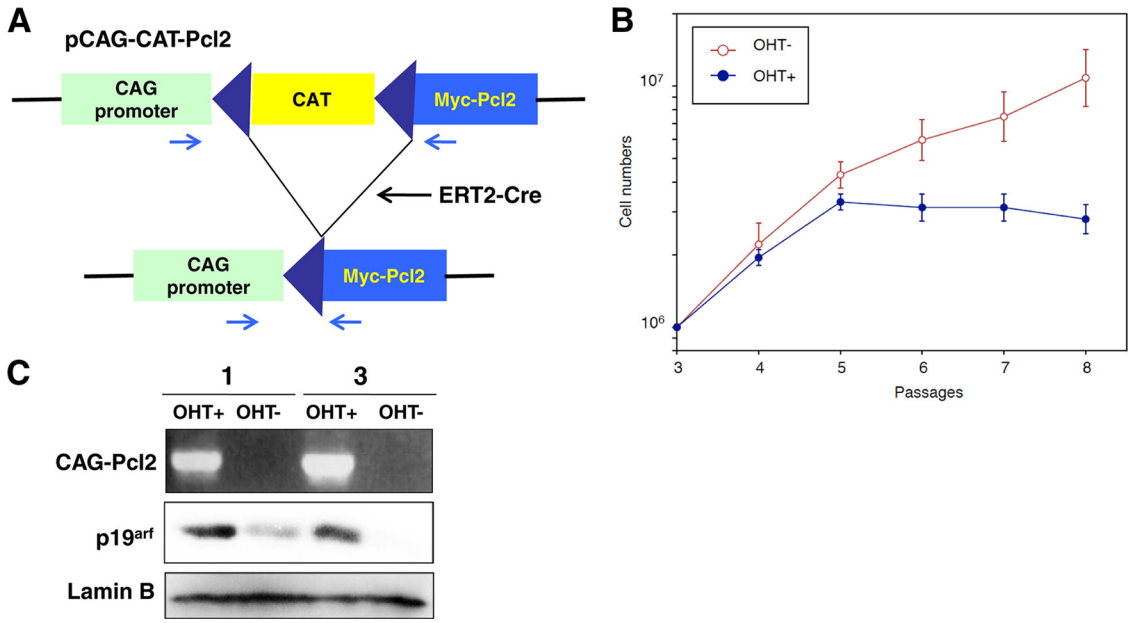

FIG. 7. Pcl2 regulates cellular senescence through *Cdkn2a*. (A) Schematic representation of the transgene to overexpress Myc-tagged Pcl2 in a Cre recombinase-dependent manner. Briefly, the *lacZ* gene in CAG-CAT-Z (4) was replaced by Myc-tagged Pcl2. Pcl2 expression is therefore induced by deletion of chloramphenicol acetyltransferase (CAT) gene cassette placed between two *loxP* sites (shown by arrows) by Cre recombinase. A transgenic line harboring this inducible construct was bred with another transgenic line expressing ERT2-Cre to generate MEFs in which Pcl2 could be expressed upon 4-hydroxytamoxifen ([OHT] 0.5 μM) treatment. The location of primers used to assess deletion of the CAT gene cassette is shown. (B) Impact of Myc-tagged Pcl2 on replicative senescence as revealed by a modified 3T9 assay. Double transgenic MEFs were treated by 0.5 μM tamoxifen at passage 3 (OHT+), and growth rate was examined after the treatment by using untreated MEFs as a control (OHT−). Overexpression of Pcl2 (OHT+) clearly induced premature proliferation arrest. (C) Induction of $p19^{arf}$ expression upon deletion of the CAT gene in two different MEF lines harboring double transgenes. The top panel is an assessment of tamoxifen-induced recombination of the transgene, the middle shows results of Western blotting for $p19^{arf}$ expression, and the bottom shows results of Western blotting for lamin B expression as dose controls.

Pcl2 for PRC2 to exert its functions in *Hox* repression. Therefore, Pcl2 is a functional component of PRC2. It is also noteworthy, however, that the *Pcl2* mutation affects PRC1-mediated repression of *Hox* genes as manifested by genetic interactions between *Pcl2* and *Mel18* or *Phc2* although local depositions of H3K27me3 or Ring1B were not significantly altered in the *Pcl2* mutants. Although the detailed underlying mechanisms are as yet unclear, our results strongly indicate that Pcl2 cooperates with both PRC2 and PRC1 to regulate the expression of *Hox* cluster genes during axial development (Fig. 8C). In contrast, Pcl2 activates the expression of *Cdkn2a* genes once primary fibroblasts become predisposed to stress-induced senescence (Fig. 8C). In this case, Pcl2 could primarily act by suppressing the local catalytic activity of PRC2, which may in turn enable bypassing of PRC1-mediated repression. Taken together, these results show that Pcl2 is required to modify the functional engagement of PRC2 and PRC1 complexes, presumably by sensing cellular circumstances. However, we could not unequivocally exclude the possibility that Pcl2 might have functions independent of PRC2 in regulation of cellular senescence.

Molecular mechanisms that link Pcl2 to such cellular circumstances remain as yet unknown. One intriguing possibility is that Pcl2 might recognize local chromatin cues by its Tudor domain and/or PHD fingers. By using the $Pcl2^{\Delta}$ allele, we have shown a requirement for the 67- and 55-kDa isoforms of Pcl2 to mediate *Hox* repression in developing embryos and *Cdkn2a* activation in MEFs. Based on other recent studies, both Tudor and PHD finger domains have emerged as binding modules for methylated histone tails (7, 26, 34). Particularly, the PHD fingers of Pcl2 are predicted to recognize unmethylated or trimethylated histone H3K4 based on their respective primary structures (42, 52, 60, 65). Polycomb target genes, including *Hox* genes, are known to be bivalently marked by H3K27me3 and H3K4me3 in several cell types. Pcl2 may contribute to the *Hox* regulation via its recognition of the methylation status of H3K4 in developing embryos. In addition to detection of the methylation status of histone tails, Tudor and PHD finger domains have also been shown to contribute to recognition of RNA and phosphatidylinositols, respectively (7, 22, 26). We thus postulate that Pcl2 might use a combination of the Tudor domain and PHD fingers to discern chromatin circumstances and affect local activity of PRC2 via physical interaction. Identification of ligands for the Pcl2 Tudor domain and PHD fingers will be necessary to fully clarify this issue.

It is well known that the expression of *Hox* genes continues to be dynamically regulated in developing tissues after the initial establishment of their early expression domains (16). This implies that Polycomb-dependent *Hox* repression is plastic with the potential to be reactivated, presumably by various differentiation cues. In line with this, PRC1 has been shown to be linked to inductive signals mediating cellular differentiation, survival, and/or proliferation in cerebellar progenitors and ES cells (18, 39). Moreover, recent studies demonstrate that dy-

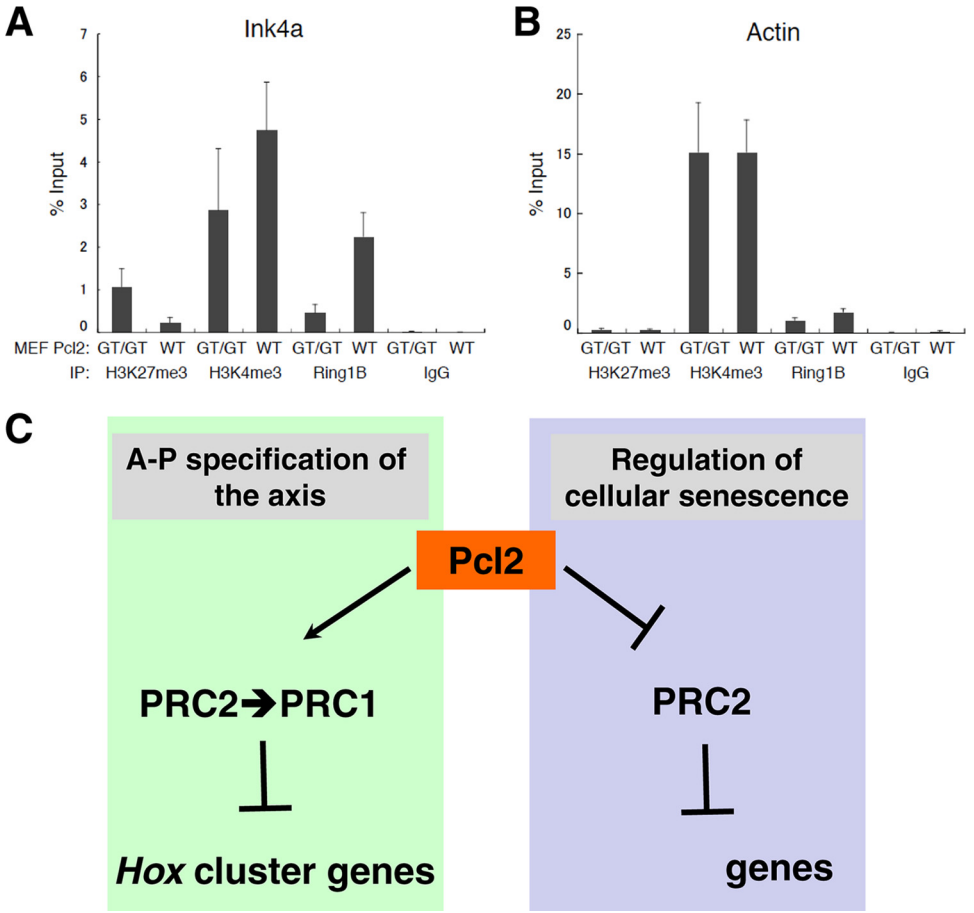

FIG. 8. The role of Pcl2 for PRC2 and PRC1. (A and B) Enrichment of H3K27me3, H3K4me3, and Ring1B at the $p16^{Ink4a}$ promoter region was determined by ChIP and site-specific real-time PCR. The β-actin promoter was used as a control. (C) A model for Pcl2 functions during A-P specification of the axis and stress-induced cellular senescence. In developing embryos, Pcl2 is a functional component of PRC2 and also functionally cooperates with PRC1 to mediate repression of *Hox* cluster genes. Upon replicative stress, Pcl2 activates *Cdkn2a* expression and suppresses cellular senescence, likely by suppressing the catalytic activity of PRC2 at the *Cdkn2a* locus.

namic regulation of Polycomb activity orchestrated by the Jumonji (or Jarid2) protein included in PRC2 balances self-renewal and differentiation of ES cells (58). In this regard, it is worthy of note that Pcl2 is copurified with Jumonji (41). Pcl2, in collaboration with proteins such as Jumonji, could act as a module that mediates such plasticity of Polycomb repression by discerning chromatin circumstances induced by differentiation cues.

ACKNOWLEDGMENT

This project was in part supported by Genome Network Project from the Ministry of Education, Culture, Sports, Science and Technology of the Japanese Government (H.K.).

REFERENCES

1. **Akasaka, T., M. Kanno, R. Balling, M. A. Mieza, M. Taniguchi, and H. Koseki.** 1996. A role for mel-18, a Polycomb group-related vertebrate gene, during the anteroposterior specification of the axial skeleton. Development **122:**1513–1522.
2. **Akasaka, T., M. van Lohuizen, N. van der Lugt, Y. Mizutani-Koseki, M. Kanno, M. Taniguchi, M. Vidal, M. Alkema, A. Berns, and H. Koseki.** 2001. Mice doubly deficient for the Polycomb group genes Mel18 and Bmi1 reveal synergy and requirement for maintenance but not initiation of Hox gene expression. Development **128:**1587–1597.
3. **Altschul, S. F., W. Gish, W. Miller, E. W. Myers, and D. J. Lipman.** 1990. Basic local alignment search tool. J. Mol. Biol. **215:**403–410.
4. **Araki, K., M. Araki, J. Miyazaki, and P. Vassalli.** 1995. Site-specific recombination of a transgene in fertilized eggs by transient expression of Cre recombinase. Proc. Natl. Acad. Sci. U. S. A. **92:**160–164.
5. **Atsuta, T., S. Fujimura, H. Moriya, M. Vidal, T. Akasaka, and H. Koseki.** 2001. Production of monoclonal antibodies against mammalian Ring1B proteins. Hybridoma **20:**43–46.
6. **Bel, S., N. Core, M. Djabali, K. Kieboom, N. Van der Lugt, M. J. Alkema, and M. Van Lohuizen.** 1998. Genetic interactions and dosage effects of Polycomb group genes in mice. Development **125:**3543–3551.
7. **Bernstein, E., and C. D. Allis.** 2005. RNA meets chromatin. Genes Dev. **19:**1635–1655.
8. **Boyer, L. A., K. Plath, J. Zeitlinger, T. Brambrink, L. A. Medeiros, T. I. Lee, S. S. Levine, M. Wernig, A. Tajonar, M. K. Ray, G. W. Bell, A. P. Otte, M. Vidal, D. K. Gifford, R. A. Young, and R. Jaenisch.** 2006. Polycomb complexes repress developmental regulators in murine embryonic stem cells. Nature **441:**349–353.
9. **Cao, R., Y. Tsukada, and Y. Zhang.** 2005. Role of Bmi-1 and Ring1A in H2A ubiquitylation and Hox gene silencing. Mol. Cell **20:**845–854.
10. **Cao, R., H. Wang, J. He, H. Erdjument-Bromage, P. Tempst, and Y. Zhang.** 2008. Role of hPHF1 in H3K27 methylation and Hox gene silencing. Mol. Cell. Biol. **28:**1862–1872.
11. **Cao, R., L. Wang, H. Wang, L. Xia, H. Erdjument-Bromage, P. Tempst, R. S. Jones, and Y. Zhang.** 2002. Role of histone H3 lysine 27 methylation in Polycomb-group silencing. Science **298:**1039–1043.
12. **Coulson, M., S. Robert, H. J. Eyre, and R. Saint.** 1998. The identification and localization of a human gene with sequence similarity to Polycomblike of *Drosophila melanogaster*. Genomics **48:**381–383.
13. **Czermin, B., R. Melfi, D. McCabe, V. Seitz, A. Imhof, and V. Pirrotta.** 2002. *Drosophila* enhancer of Zeste/ESC complexes have a histone H3 methyl-

transferase activity that marks chromosomal Polycomb sites. Cell **111:**185–196.
14. **de Napoles, M., J. E. Mermoud, R. Wakao, Y. A. Tang, M. Endoh, R. Appanah, T. B. Nesterova, J. Silva, A. P. Otte, M. Vidal, H. Koseki, and N. Brockdorff.** 2004. Polycomb group proteins Ring1A/B link ubiquitylation of histone H2A to heritable gene silencing and X inactivation. Dev. Cell **7:**663–676.
15. **Dignam, J. D., R. M. Lebovitz, and R. G. Roeder.** 1983. Accurate transcription initiation by RNA polymerase II in a soluble extract from isolated mammalian nuclei. Nucleic Acids Res. **11:**1475–1489.
16. **Duboule, D.** 1995. Vertebrate Hox genes and proliferation: an alternative pathway to homeosis? Curr. Opin. Genet. Dev. **5:**525–528.
17. **Duncan, I. M.** 1982. Polycomblike: a gene that appears to be required for the normal expression of the bithorax and antennapedia gene complexes of *Drosophila melanogaster*. Genetics **102:**49–70.
18. **Endoh, M., T. A. Endo, T. Endoh, Y. Fujimura, O. Ohara, T. Toyoda, A. P. Otte, M. Okano, N. Brockdorff, M. Vidal, and H. Koseki.** 2008. Polycomb group proteins Ring1A/B are functionally linked to the core transcriptional regulatory circuitry to maintain ES cell identity. Development **135:**1513–1524.
19. **Eskeland, R., M. Leeb, G. R. Grimes, C. Kress, S. Boyle, D. Sproul, N. Gilbert, Y. Fan, A. I. Skoultchi, A. Wutz, and W. A. Bickmore.** 2010. Ring1B compacts chromatin structure and represses gene expression independent of histone ubiquitination. Mol. Cell **38:**452–464.
20. **Francis, N. J., A. J. Saurin, Z. Shao, and R. E. Kingston.** 2001. Reconstitution of a functional core polycomb repressive complex. Mol. Cell **8:**545–556.
21. **Fujimura, Y., K. Isono, M. Vidal, M. Endoh, H. Kajita, Y. Mizutani-Koseki, Y. Takihara, M. van Lohuizen, A. Otte, T. Jenuwein, J. Deschamps, and H. Koseki.** 2006. Distinct roles of Polycomb group gene products in transcriptionally repressed and active domains of Hoxb8. Development **133:**2371–2381.
22. **Gozani, O., P. Karuman, D. R. Jones, D. Ivanov, J. Cha, A. A. Lugovskoy, C. L. Baird, H. Zhu, S. J. Field, S. L. Lessnick, J. Villasenor, B. Mehrotra, J. Chen, V. R. Rao, J. S. Brugge, C. G. Ferguson, B. Payrastre, D. G. Myszka, L. C. Cantley, G. Wagner, N. Divecha, G. D. Prestwich, and J. Yuan.** 2003. The PHD finger of the chromatin-associated protein ING2 functions as a nuclear phosphoinositide receptor. Cell **114:**99–111.
23. **Hamer, K. M., R. G. Sewalt, J. L. den Blaauwen, T. Hendrix, D. P. Satijn, and A. P. Otte.** 2002. A panel of monoclonal antibodies against human polycomb group proteins. Hybrid. Hybridomics **21:**245–252.
24. **Hansen, J., T. Floss, P. Van Sloun, E. M. Fuchtbauer, F. Vauti, H. H. Arnold, F. Schnutgen, W. Wurst, H. von Melchner, and P. Ruiz.** 2003. A large-scale, gene-driven mutagenesis approach for the functional analysis of the mouse genome. Proc. Natl. Acad. Sci. U. S. A. **100:**9918–9922.
25. **Hong, Z., J. Jiang, L. Lan, S. Nakajima, S. Kanno, H. Koseki, and A. Yasui.** 2008. A polycomb group protein, PHF1, is involved in the response to DNA double-strand breaks in human cell. Nucleic Acids Res. **36:**2939–2947.
26. **Huyen, Y., O. Zgheib, R. A. Ditullio, Jr., V. G. Gorgoulis, P. Zacharatos, T. J. Petty, E. A. Sheston, H. S. Mellert, E. S. Stavridi, and T. D. Halazonetis.** 2004. Methylated lysine 79 of histone H3 targets 53BP1 to DNA double-strand breaks. Nature **432:**406–411.
27. **Inouye, C., P. Remondelli, M. Karin, and S. Elledge.** 1994. Isolation of a cDNA encoding a metal response element binding protein using a novel expression cloning procedure: the one hybrid system. DNA Cell Biol. **13:**731–742.
28. **Isono, K., Y. Fujimura, J. Shinga, M. Yamaki, J. O. Wang, Y. Takihara, Y. Murahashi, Y. Takada, Y. Mizutani-Koseki, and H. Koseki.** 2005. Mammalian polyhomeotic homologues Phc2 and Phc1 act in synergy to mediate polycomb repression of *Hox* genes. Mol. Cell. Biol. **25:**6694–6706.
29. **Isono, K., Y. Mizutani-Koseki, T. Komori, M. S. Schmidt-Zachmann, and H. Koseki.** 2005. Mammalian polycomb-mediated repression of Hox genes requires the essential spliceosomal protein Sf3b1. Genes Dev. **19:**536–541.
30. **Jacobs, J. J., K. Kieboom, S. Marino, R. A. DePinho, and M. van Lohuizen.** 1999. The oncogene and Polycomb-group gene *bmi-1* regulates cell proliferation and senescence through the *ink4a* locus. Nature **397:**164–168.
31. **Kamijo, T., F. Zindy, M. F. Roussel, D. E. Quelle, J. R. Downing, R. A. Ashmun, G. Grosveld, and C. J. Sherr.** 1997. Tumor suppression at the mouse INK4a locus mediated by the alternative reading frame product p19ARF. Cell **91:**649–659.
32. **Kawakami, S., K. Mitsunaga, Y. Y. Kikuti, A. Ando, H. Inoko, K. Yamamura, and K. Abe.** 1998. Tctex3, related to *Drosophila* polycomblike, is expressed in male germ cells and mapped to the mouse t-complex. Mamm. Genome **9:**874–880.
33. **Kennison, J. A., and J. W. Tamkun.** 1988. Dosage-dependent modifiers of polycomb and antennapedia mutations in *Drosophila*. Proc. Natl. Acad. Sci. U. S. A. **85:**8136–8140.
34. **Kim, J., J. Daniel, A. Espejo, A. Lake, M. Krishna, L. Xia, Y. Zhang, and M. T. Bedford.** 2006. Tudor, MBT and chromo domains gauge the degree of lysine methylation. EMBO Rep. **7:**397–403.
35. **King, I. F., N. J. Francis, and R. E. Kingston.** 2002. Native and recombinant Polycomb group complexes establish a selective block to template accessibility to repress transcription in vitro. Mol. Cell. Biol. **22:**7919–7928.
36. **Kitaguchi, T., K. Nakata, T. Nagai, J. Aruga, and K. Mikoshiba.** 2001. *Xenopus* Polycomblike 2 (XPcl2) controls anterior to posterior patterning of the neural tissue. Dev. Genes Evol. **211:**309–314.
37. **Ku, M., R. P. Koche, E. Rheinbay, E. M. Mendenhall, M. Endoh, T. S. Mikkelsen, A. Presser, C. Nusbaum, X. Xie, A. S. Chi, M. Adli, S. Kasif, L. M. Ptaszek, C. A. Cowan, E. S. Lander, H. Koseki, and B. E. Bernstein.** 2008. Genomewide analysis of PRC1 and PRC2 occupancy identifies two classes of bivalent domains. PLoS Genet. **4:**e1000242.
38. **Lee, T. I., R. G. Jenner, L. A. Boyer, M. G. Guenther, S. S. Levine, R. M. Kumar, B. Chevalier, S. E. Johnstone, M. F. Cole, K. Isono, H. Koseki, T. Fuchikami, K. Abe, H. L. Murray, J. P. Zucker, B. Yuan, G. W. Bell, E. Herbolsheimer, N. M. Hannett, K. Sun, D. T. Odom, A. P. Otte, T. L. Volkert, D. P. Bartel, D. A. Melton, D. K. Gifford, R. Jaenisch, and R. A. Young.** 2006. Control of developmental regulators by Polycomb in human embryonic stem cells. Cell **125:**301–313.
39. **Leung, C., M. Lingbeek, O. Shakhova, J. Liu, E. Tanger, P. Saremaslani, M. Van Lohuizen, and S. Marino.** 2004. Bmi1 is essential for cerebellar development and is overexpressed in human medulloblastomas. Nature **428:**337–341.
40. **Levine, S. S., A. Weiss, H. Erdjument-Bromage, Z. Shao, P. Tempst, and R. E. Kingston.** 2002. The core of the Polycomb repressive complex is compositionally and functionally conserved in flies and humans. Mol. Cell. Biol. **22:**6070–6078.
41. **Li, G., R. Margueron, M. Ku, P. Chambon, B. E. Bernstein, and D. Reinberg.** 2010. Jarid2 and PRC2, partners in regulating gene expression. Genes Dev. **24:**368–380.
42. **Li, H., S. Ilin, W. Wang, E. M. Duncan, J. Wysocka, C. D. Allis, and D. J. Patel.** 2006. Molecular basis for site-specific read-out of histone H3K4me3 by the BPTF PHD finger of NURF. Nature **442:**91–95.
43. **Lonie, A., R. D'Andrea, R. Paro, and R. Saint.** 1994. Molecular characterisation of the Polycomblike gene of *Drosophila melanogaster*, a trans-acting negative regulator of homeotic gene expression. Development **120:**2629–2636.
44. **Mikkelsen, T. S., M. Ku, D. B. Jaffe, B. Issac, E. Lieberman, G. Giannoukos, P. Alvarez, W. Brockman, T. K. Kim, R. P. Koche, W. Lee, E. Mendenhall, A. O'Donovan, A. Presser, C. Russ, X. Xie, A. Meissner, M. Wernig, R. Jaenisch, C. Nusbaum, E. S. Lander, and B. E. Bernstein.** 2007. Genome-wide maps of chromatin state in pluripotent and lineage-committed cells. Nature **448:**553–560.
45. **Mortazavi, A., B. A. Williams, K. McCue, L. Schaeffer, and B. Wold.** 2008. Mapping and quantifying mammalian transcriptomes by RNA-Seq. Nat. Methods **5:**621–628.
46. **Muller, J., C. M. Hart, N. J. Francis, M. L. Vargas, A. Sengupta, B. Wild, E. L. Miller, M. B. O'Connor, R. E. Kingston, and J. A. Simon.** 2002. Histone methyltransferase activity of a *Drosophila* Polycomb group repressor complex. Cell **111:**197–208.
47. **Nekrasov, M., T. Klymenko, S. Fraterman, B. Papp, K. Oktaba, T. Kocher, A. Cohen, H. G. Stunnenberg, M. Wilm, and J. Muller.** 2007. Pcl-PRC2 is needed to generate high levels of H3-K27 trimethylation at Polycomb target genes. EMBO J. **26:**4078–4088.
48. **O'Carroll, D., S. Erhardt, M. Pagani, S. C. Barton, M. A. Surani, and T. Jenuwein.** 2001. The *Polycomb*-group gene *Ezh2* is required for early mouse development. Mol. Cell. Biol. **21:**4330–4336.
49. **O'Connell, S., L. Wang, S. Robert, C. A. Jones, R. Saint, and R. S. Jones.** 2001. Polycomblike PHD fingers mediate conserved interaction with enhancer of zeste protein. J. Biol. Chem. **276:**43065–43073.
50. **Paro, R.** 1995. Propagating memory of transcriptional states. Trends Genet. **11:**295–297.
51. **Pasini, D., A. P. Bracken, M. R. Jensen, E. Lazzerini Denchi, and K. Helin.** 2004. Suz12 is essential for mouse development and for EZH2 histone methyltransferase activity. EMBO J. **23:**4061–4071.
52. **Pena, P. V., F. Davrazou, X. Shi, K. L. Walter, V. V. Verkhusha, O. Gozani, R. Zhao, and T. G. Kutateladze.** 2006. Molecular mechanism of histone H3K4me3 recognition by plant homeodomain of ING2. Nature **442:**100–103.
53. **Pirrotta, V.** 1997. PcG complexes and chromatin silencing. Curr. Opin. Genet. Dev. **7:**249–258.
54. **Sakai, K., and J. Miyazaki.** 1997. A transgenic mouse line that retains Cre recombinase activity in mature oocytes irrespective of the *cre* transgene transmission. Biochem. Biophys. Res. Commun. **237:**318–324.
55. **Sarma, K., R. Margueron, A. Ivanov, V. Pirrotta, and D. Reinberg.** 2008. Ezh2 requires PHF1 to efficiently catalyze H3 lysine 27 trimethylation in vivo. Mol. Cell. Biol. **28:**2718–2731.
56. **Savla, U., J. Benes, J. Zhang, and R. S. Jones.** 2008. Recruitment of *Drosophila* Polycomb-group proteins by Polycomblike, a component of a novel protein complex in larvae. Development **135:**813–817.
57. **Shao, Z., F. Raible, R. Mollaaghababa, J. R. Guyon, C. T. Wu, W. Bender, and R. E. Kingston.** 1999. Stabilization of chromatin structure by PRC1, a Polycomb complex. Cell **98:**37–46.
58. **Shen, X., W. Kim, Y. Fujiwara, M. D. Simon, Y. Liu, M. R. Mysliwiec, G. C. Yuan, Y. Lee, and S. H. Orkin.** 2009. Jumonji modulates polycomb activity and self-renewal versus differentiation of stem cells. Cell **139:**1303–1314.

59. **Sherr, C. J., and R. A. DePinho.** 2000. Cellular senescence: mitotic clock or culture shock? Cell **102:**407–410.
60. **Shi, X., T. Hong, K. L. Walter, M. Ewalt, E. Michishita, T. Hung, D. Carney, P. Pena, F. Lan, M. R. Kaadige, N. Lacoste, C. Cayrou, F. Davrazou, A. Saha, B. R. Cairns, D. E. Ayer, T. G. Kutateladze, Y. Shi, J. Cote, K. F. Chua, and O. Gozani.** 2006. ING2 PHD domain links histone H3 lysine 4 methylation to active gene repression. Nature **442:**96–99.
61. **Shumacher, A., C. Faust, and T. Magnuson.** 1996. Positional cloning of a global regulator of anterior-posterior patterning in mice. Nature **383:**250–253.
62. **Tie, F., J. Prasad-Sinha, A. Birve, A. Rasmuson-Lestander, and P. J. Harte.** 2003. A 1-megadalton ESC/E(Z) complex from *Drosophila* that contains polycomblike and RPD3. Mol. Cell. Biol. **23:**3352–3362.
63. **Walker, E., W. Y. Chang, J. Hunkapiller, G. Cagney, K. Garcha, J. Torchia, N. J. Krogan, J. F. Reiter, and W. L. Stanford.** 2010. Polycomb-like 2 associates with PRC2 and regulates transcriptional networks during mouse embryonic stem cell self-renewal and differentiation. Cell Stem Cell **6:**153–166.
64. **Wang, H., L. Wang, H. Erdjument-Bromage, M. Vidal, P. Tempst, R. S. Jones, and Y. Zhang.** 2004. Role of histone H2A ubiquitination in Polycomb silencing. Nature **431:**873–878.
65. **Wang, S., F. He, W. Xiong, S. Gu, H. Liu, T. Zhang, X. Yu, and Y. Chen.** 2007. Polycomblike-2-deficient mice exhibit normal left-right asymmetry. Dev. Dyn. **236:**853–861.
66. **Wang, S., X. Yu, T. Zhang, X. Zhang, Z. Zhang, and Y. Chen.** 2004. Chick Pcl2 regulates the left-right asymmetry by repressing Shh expression in Hensen's node. Development **131:**4381–4391.